Phonon quasiparticles and anharmonic perturbation theory tested by molecular dynamics on a model system

Tao Sun,[1,2,3,*] Xiao Shen,[3,†] and Philip B. Allen[3,‡]
[1]*DEMOCRITOS Theory@Elettra group, CNR-Istituto Officina dei Materiali (IOM), Area Science Park SS14, Km 163, 5 Basovizza, I-34012 Trieste, Italy*
[2]*Scuola Internazionale Superiore di Studi Avanzati (SISSA), via Bonomea 265, I-34136 Trieste, Italy*
[3]*Department of Physics and Astronomy, Stony Brook University, Stony Brook, New York 11794, USA*
(Received 5 August 2010; published 13 December 2010)

Vibrational spectra and thermal properties of a two-dimensional triangular lattice, where first-neighbor atoms interact with a Lennard-Jones potential, are calculated using both classical molecular dynamics (MD) and leading-order anharmonic perturbation theory (PT). The phonon quasiparticle spectra (QPS), obtained nonperturbatively through MD, depend linearly on T at low temperatures and are in good agreement with the QPS calculated by PT. However, noticeable deviations from the linear T dependence are observed at high T, which are attributed to higher order anharmonic effects. We find that when the QPS obtained by leading-order PT are used in the quasiparticle entropy formula, the first-order anharmonic corrections to the thermal properties are correctly generated. Higher order anharmonic corrections are also described, if one uses the nonperturbative QPS obtained from MD. The success of quasiparticle theory is somewhat surprising in light of strong deviations of the thermal conductivity from Peierls-Boltzmann theory, as found in the companion paper.

DOI: 10.1103/PhysRevB.82.224304 PACS number(s): 65.40.−b, 63.20.D−, 63.20.kg

I. INTRODUCTION

Anharmonic interactions vary a lot in solids. Silicon remains quite harmonic to high T (allowing thermal conductivity to remain high) (Ref. 1) while CuCl is sufficiently anharmonic that phonon quasiparticles are destroyed by room temperature.[2] This paper uses high T molecular-dynamics (MD) modeling (in the regime where quantum effects are unimportant) to examine the reliability of the quasiparticle picture and of anharmonic perturbation theory (PT) for the vibrational spectrum and the thermodynamics. The following paper[3] does the same for thermal conductivity. Such examinations have been done before.[4–6] There are two reasons for further work. First, anharmonic interactions are not "universal." Their magnitude differs among solids so a new model is worth examining. Second, the two-dimensional (2D) model we use is sufficiently simple that many nonperturbative calculations can be done quickly and with smaller numerical noise than has been achieved in three-dimensional models and compared with accurate perturbative calculations.

Consider the analogies between electrons in solids and lattice vibrations. In the case of electrons, the classical Drude model of noninteracting electrons became much more useful when quantized by Sommerfeld. Bloch provided the generalization to bands in real crystals and Landau provided the quasiparticle picture, which showed how to retain a modified Bloch picture in spite of electron-electron Coulomb interactions. The central idea of the quasiparticle picture is the distribution function f_k, whose evolution is governed by the Bloch-Boltzmann equation (with Coulomb interactions included). We lack a full understanding of how strong Coulomb interactions destroy quasiparticles. The "pseudogap" state seems to evolve continuously from Landau quasiparticles while Mott insulators and fractional quantum-Hall states have no adiabatic connection to Landau quasiparticles.

Lattice vibrations were quantized by Einstein, discovered to propagate and carry heat by Debye, and given modern crystalline properties by Born and von Karman. Quantum mechanics encourages the particle interpretation (and the name "phonon") but this interpretation remains useful even in a purely classical context as used here. The distribution function n_k, evolving according to the Peierls-Boltzmann equation, is again central. Phonon quasiparticles, when not destroyed by anharmonicity, are nice analogs of Landau electron quasiparticles. Anharmonic interactions between phonons are just as challenging for PT as are Coulomb interactions. Usually no discontinuously different state occurs although low T helium liquids are exceptions. Theory has the big advantage in the phonon case that classical theory is usually adequate at higher T. Classical MD modeling is much easier than quantum Monte Carlo modeling. This paper and its companion[3] (hereafter called II) use MD to examine strong anharmonic interactions in a regime where they cause breakdown of low-order PT, the Peierls-Boltzmann equation, and potentially the quasiparticle picture.

The model studied here is the 2D triangular lattice with a nearest neighbor only Lennard-Jones (LJ) potential. The restriction to nearest neighbor only makes both PT and MD calculations easier. Our numerical results in II show a factor of 2 deviation from the perturbative Boltzmann result for thermal conductivity. The results of the present paper show a surprisingly mild influence of anharmonicity on the quasiparticle spectrum and thermodynamics.

II. QUASIPARTICLE THEORY

The quantum numbers $\mathbf{k},s$ of a phonon quasiparticle will be denoted for short as k. The symbol n_k denotes the number of phonons in-state k or the distribution function. Entropy measures the multiplicity of ways of distributing quasiparticles. Using the notion that the number of phonons in-state k

can be any non-negative integer, an entropy formula follows:[7]

$$S_{\mathrm{QP}} = k_B \sum_k [(n_k+1)\ln(n_k+1) - n_k \ln n_k], \tag{1}$$

Maximizing S_{QP} subject to constant total quasiparticle energy $E_{\mathrm{QP}}=\Sigma_k \hbar\omega_k n_k$, the optimum distribution function is the Bose-Einstein distribution $n_k=[\exp(\beta\hbar\omega_k)-1]^{-1}$, where the Lagrange multiplier β is interpreted as $1/k_BT$. Just as the distribution function is the central idea of quasiparticle theory, the entropy plays a special role. If quasiparticle energy evolves as a function of temperature, the entropy formula, Eq. (1) with temperature-dependent phonon energies in the Bose-Einstein distribution, is valid to second order in anharmonic PT (Refs. 8–10) and probably somewhat beyond.[11] Harmonic formulas such as the Helmholtz free energy

$$F_{\mathrm{H}} = \frac{1}{2}\sum_k \hbar\omega_k + k_BT\sum_k \ln[1-\exp(-\hbar\omega_k/k_BT)] \tag{2}$$

are not correct when the T-dependent quasiparticle energy is included.[9,12,13] If, however, the source of T dependence is a temperature-dependent volume $V(T)$, so that $\omega_k[V(T)]$ acquires a T dependence only through thermal expansion, then the harmonic free-energy formula becomes the basis of quasiharmonic (QHA) theory, which has some successes.[14] However, lattice expansion is probably never the dominant source of temperature dependence of quasiparticle energies.[15,16] One outcome of our work is that we can test these ideas.

There is an alternative route to the quasiparticle entropy worth mentioning. Under an applied temperature gradient, the distribution function is altered by drift and scattering. Under the assumption that the equation is closed (no two phonon or higher order distribution functions are needed), the evolution equation for the distribution function is a Boltzmann equation (first derived by Peierls[17]). This equation has the beautiful property (quantum generalization of Boltzmann H-theorem, first announced by Pauli[18]) that the entropy formula, Eq. (1), never decreases in time and has a unique stationary solution, when n_k is the Bose-Einstein distribution.

The quasiparticle picture can fail. We will show in II that the thermal conductivity of our model shows signs of such a failure. However, the quasiparticle properties discussed in the present paper turn out to be surprisingly robust.

III. 2D TRIANGULAR LATTICE, HARMONIC LIMIT

We choose a 2D triangular lattice as the model system, which is illustrated in Fig. 1. The basis vectors **a** and **b** have the same length $a=|\mathbf{a}|$ and are 120° from each other. In Cartesian coordinates $\mathbf{a}=a(1/2,-\sqrt{3}/2)$ and $\mathbf{b}=a(1/2,\sqrt{3}/2)$. It is convenient to define also a third vector $\mathbf{c}=a(-1,0)$, which lies at 120° to **a** and **b**. In this lattice, every atom is at a lattice point. An atom at $\mathbf{R}_i$ has six nearest neighbors at positions $\mathbf{R}_j=\mathbf{R}_i\pm\mathbf{a},\pm\mathbf{b},\pm\mathbf{c}$. This serves as a model crystal with just enough complexity to serve as a model for real crystals but sufficient simplicity to enable some simple formulas and rapid computer modeling. To keep things as simple as possible, consider the atoms as point particles of mass m, interacting only with six designated nearest neighbors by a central potential $\phi(r_{ij})$, where r_{ij}, defined as $r_{ij}=|\mathbf{r}_i-\mathbf{r}_j|$, is the distance between two particles i and j. The total potential energy of the lattice can be written as

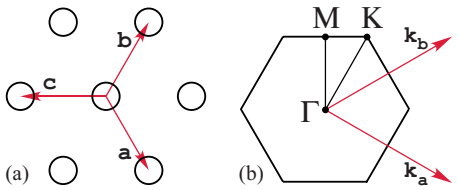

FIG. 1. (Color online) (a) 2D triangular lattice. (b) Brillouin zone of the 2D triangular lattice.

$$\Phi = \frac{1}{2}\sum_i \sum_j^{\mathrm{NN}} \phi(r_{ij}). \tag{3}$$

We choose the potential to be the Lennard-Jones potential

$$\phi_{\mathrm{LJ}}(r) = \epsilon\left[\left(\frac{\sigma}{r}\right)^{12} - 2\left(\frac{\sigma}{r}\right)^{6}\right]. \tag{4}$$

There is no large r cutoff but also no long-range force since atoms interact only with designated nearest neighbors which do not stray until $k_BT>\epsilon$. The minimum value $\phi_{\mathrm{min}}=-\epsilon$ is at $r=\sigma$. The variables (m,σ,ϵ) can be chosen as the units of mass, length, and energy. For a pair of Ar atoms, $\sigma=3.87$ Å, $\epsilon=113.7$ K, and the time unit $\sigma\sqrt{m/\epsilon}$ is 2.515 ps.[19] We keep the volume fixed and the lattice constant of our crystal is $a=\sigma=1$. The classical ground state is a triangular lattice with atoms at sites $\mathbf{R}_i=m\mathbf{a}+n\mathbf{b}$. The ground-state energy is $-3N\epsilon$, where N is the number of particles.

Figure 2 shows the harmonic phonon spectrum and group velocities, using the formula shown in the Appendix. There are two branches both acoustic. Symmetry requires the 2D triangular lattice to be elastically isotropic. Taking the long-wavelength limit of Eq. (A6), we find the longitudinal and transverse sound velocities are independent of the direction of **k** with values $mv_{\mathrm{L}}^2/\sigma^2=9\phi''/8$ and $mv_{\mathrm{T}}^2/\sigma^2=3\phi''/8$, after setting $\phi'=0$. These numbers are consistent with the elastic constants determined by differentiating the total potential energy Φ with respect to infinitesimal strains.[20] Due to symmetry, there are only two independent nonzero components, $C_{11}=C_{22}=9\phi''/(4\sqrt{3})$ and $C_{12}=C_{66}=3\phi''/(4\sqrt{3})$. When T is low and anharmonic phonon-phonon interactions are weak, phonon frequencies should be close to the harmonic ones. Indeed we find that phonon frequencies obtained from MD at the lowest temperature we explore, $T=0.05$, agree very well with the harmonic frequencies.

Figure 3 shows the dispersion of the mode-Grüneisen parameter γ_k. We find that γ_k is in the range of 4.5~5.17 with a mean value $\bar{\gamma}$ of 4.9. The Grüneisen parameter $\bar{\gamma}$ has long served as a convenient measure of anharmonicity. For crystalline Ar, $\bar{\gamma}=2.7$ at 0 K.[21] The large $\bar{\gamma}$ observed in our 2D system indicates that it is strongly anharmonic.

It has been known for a long time[22–25] that a two-dimensional crystal has diverging mean-square lattice dis-

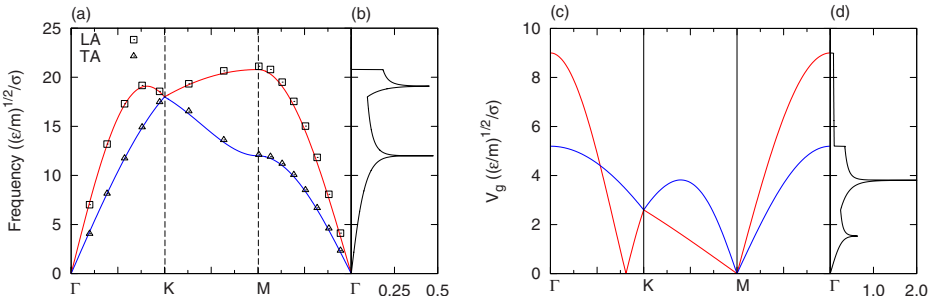

FIG. 2. (Color online) (a) Phonon dispersion curves computed from Eq. (A6). The red (light) solid line represents the LA branch, the blue (dark) solid line represents TA branch, and the dots correspond to phonon frequencies obtained from molecular dynamics at $T=0.05$. (b) Phonon density of states. (c) Group velocities v_{gk} computed from $\nabla_{\mathbf{k}}\omega_k$ and (d) distribution functions of the group velocities.

placements in the infinite crystal limit. The formula is

$$\langle u^2\rangle = \sum_k \frac{\hbar}{2mN\omega_k}(2n_k+1) \to \sum_k \frac{k_BT}{Nm\omega_k^2}, \tag{5}$$

where the last version is the classical high T limit. The sum goes over discrete wave vectors $\mathbf{k}_{mn}=(m\mathbf{k}_a+n\mathbf{k}_b)/\sqrt{N}$, where N is the number of atoms in the sample. The sum diverges as $\ln N$. This is shown in Fig. 4 for our model. Notice that not until $N\approx 10^{125}$ does the rms displacement equal the interatomic distance. Therefore it is not necessary to worry about this pathology of two dimensions. Most physical properties are affected more by the fluctuations of neighbor distances, $\langle(\mathbf{u}_1-\mathbf{u}_2)^2\rangle$. This is also shown in Fig. 4. Note that the second sum converges rapidly, being within 0.4% of the infinite limit when $N=256$. Many physical properties are thus likely to be well converged when computed by molecular dynamics on a 256 atom cell.

IV. ANHARMONIC PERTURBATION THEORY

According to many-body theory, each phonon acquires through anharmonic interactions a temperature-dependent self-energy $\Sigma(k,\omega)=\Sigma_1(k,\omega)+i\Sigma_2(k,\omega)$.[15,26] Assuming that $\Sigma_1(k,\omega)$ and $\Sigma_2(k,\omega)$ are small relative to ω_k and show little frequency dependence, one finds that $\Sigma_1(k,\omega_k)=\Delta_k$ corresponds to a frequency shift with respect to ω_k, and $\omega_k'=\omega_k+\Delta_k$ is the phonon quasiparticle frequency. Then $-\Sigma_2(k,\omega_k)=\Gamma_k$ corresponds to phonon linewidth and $\tau_k^{\mathrm{QP}}=1/2\Gamma_k$ is phonon quasiparticle relaxation time.[4] Leading order PT predicts that Δ_k and Γ_k are linear in T in the classical high-T limit.[26] These phonon quasiparticles with frequencies ω_k' and relaxation times τ_k^{QP}, provide a conceptually simple and intuitive way to study the anharmonic effects of materials at high T. Phonon quasiparticle spectra are related to thermodynamics[8–10] and quasiparticle relaxation times are related to the lattice thermal conductivity,[4,6] the subject of paper II.[3]

Define the retarded one phonon Green's function of mode k as

$$G_R(k,t) = \frac{1}{i\hbar}\langle[u_k(t),u_k^\dagger(0)]\rangle\theta(t), \tag{6}$$

where the normal-mode coordinates are $u_k=\sqrt{\hbar/(2\omega_k)}(a_k+a_{-k}^\dagger)$. From Dyson's equation, the Fourier transform $G_R(k,\omega)$ is represented in terms of phonon self-energy as

$$G_R(k,\omega) = \frac{1}{\omega^2-\omega_k^2-2\omega_k\Sigma(k,\omega)}. \tag{7}$$

Up to second order in anharmonicity, $\Sigma(k,\omega)=\Sigma_1+i\Sigma_2$ is

$$\begin{aligned}\Sigma_1(k,\omega) = &-\frac{9\hbar}{4\omega_k}\sum_{k_1k_2}\frac{|\Phi_3(k,k_1,k_2)|^2}{\omega_{k_1}\omega_{k_2}}\{(n_1+n_2+1)[1/(\omega_1+\omega_2\\ &+\omega)_p+1/(\omega_1+\omega_2-\omega)_p]+(n_2-n_1)[1/(\omega_1-\omega_2\\ &+\omega)_p-1/(\omega_2-\omega_1+\omega)_p]\}+\frac{3\hbar}{\omega_k}\sum_{k_1}\Phi_4(k,-k,k_1,\\ &-k_1)(2n_1+1)/\omega_{k_1},\end{aligned}$$

$$\begin{aligned}\Sigma_2(k,\omega) = &-\frac{9\pi\hbar}{4\omega_k}\sum_{k_1k_2}\frac{|\Phi_3(k,k_1,k_2)|^2}{\omega_{k_1}\omega_{k_2}}\{(n_1+n_2+1)[\delta(\omega_1+\omega_2\\ &-\omega)-\delta(\omega_1+\omega_2+\omega)]+(n_2-n_1)[\delta(\omega_2-\omega_1+\omega)\\ &-\delta(\omega_1-\omega_2+\omega)]\},\end{aligned} \tag{8}$$

where $n_k=a_k^\dagger a_k$ is the number of phonons in mode k. In the high-temperature limit, $n_k+1/2=k_BT/(\hbar\omega_k)$. The principle values and δ functions in Eq. (8) are approximated using[4,15,26]

$$\left(\frac{1}{\omega}\right)_{\mathrm{p}} = \frac{\omega}{\omega^2+\epsilon^2},$$

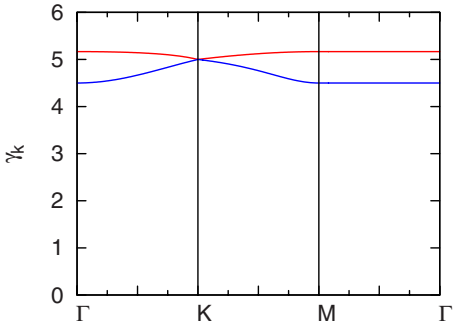

FIG. 3. (Color online) Mode Grüneisen parameter computed from Eq. (A8). The red solid line represents the LA branch and the blue solid line represents TA branch.

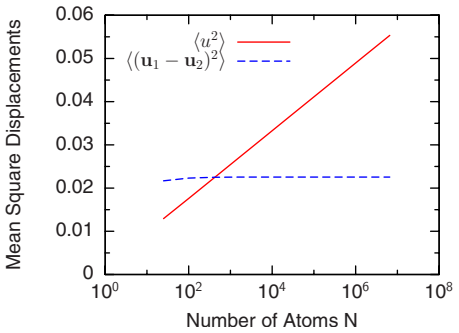

FIG. 4. (Color online) The mean-square displacement $\langle u^2 \rangle$ and mean-square nearest-neighbor fluctuation $\langle (\mathbf{u}_1 - \mathbf{u}_2)^2 \rangle$ in units σ^2, computed at $k_B T = \epsilon$, plotted against the number of atoms N in the sample. For $N > 10^2$, the numbers fit to $\langle u^2 \rangle / \sigma^2 = (0.0025 + 0.0034 \ln N)(k_B T/\epsilon)$ while $\langle (\mathbf{u}_1 - \mathbf{u}_2)^2 \rangle / \sigma^2 = 0.0235 (k_B T/\epsilon)$.

$$\delta(\omega) = \frac{1}{\pi} \frac{\epsilon}{\omega^2 + \epsilon^2}, \tag{9}$$

where the smearing parameter ϵ is set to $0.45[\sqrt{(\epsilon/m)}/\sigma]$.

V. GREEN'S FUNCTIONS FROM MOLECULAR DYNAMICS

The other way to study phonon properties is to analyze the normal-mode correlation functions obtained by classical MD. In contrast to PT, MD keeps all orders of the anharmonic interactions, and is formally exact in the classical high-T limit. We use MD results as the reference to check the validity of PT. In our MD, the boundary condition at the unit-cell boundary is periodic. Thus the system only contains phonons with wavelengths commensurate to the simulation cell. To make comparison meaningful, we carry out the PT calculation on the same $\mathbf{k}$ mesh as sampled by MD.[4] Since our $\mathbf{k}$ mesh is finite, the summation over the $\mathbf{k}$ space is always well defined.

In MD simulations, the displacement $\mathbf{u}_i$ and velocity $\mathbf{v}_i$ of each particle are determined at every time step by solving Newtonian equations. Taking the transform defined in Eq. (A9) for both $\mathbf{u}_i$ and $\mathbf{v}_i$, one obtains the instantaneous normal-mode coordinates u_k and v_k, which satisfy the relation $u_k = u_{-k}^*$ and $v_k = v_{-k}^*$. There are three types of normal-mode correlation functions, $\langle u_k^*(0) u_k(t) \rangle$, $\langle v_k^*(0) v_k(t) \rangle$, and $\langle u_k^*(0) v_k(t) \rangle$. From lattice symmetry and the fact that in equilibrium the correlation functions are stationary, it can be proven that the autocorrelations $\langle u_k^*(0) u_k(t) \rangle$ and $\langle v_k^*(0) v_k(t) \rangle$ are real and even functions while the cross correlation $\langle u_k^*(0) v_k(t) \rangle$ is a real and odd function. These correlation functions are closely related.[27] Denote their time Fourier transform as $\langle u_k^* u_k \rangle_\omega$, $\langle v_k^* v_k \rangle_\omega$, and $\langle u_k^* v_k \rangle_\omega$, we have

$$\langle v_k^* v_k \rangle_\omega = \omega^2 \langle u_k^* u_k \rangle_\omega,$$

$$\langle u_k^* v_k \rangle_\omega = -i\omega \langle u_k^* u_k \rangle_\omega,$$

$$\langle v_k^* u_k \rangle_\omega = -\langle u_k^* v_k \rangle_\omega. \tag{10}$$

Therefore only one such correlation needs to be computed. A popular choice is $\langle v_k^*(0) v_k(t) \rangle$, which is often fitted phenomenologically with a function $A_k \cos(\tilde{\omega}_k' t) e^{-\tilde{\Gamma}_k t}$.[4,28] From the equipartition theorem one expects the amplitude A_k to have little $\mathbf{k}$ dependence and to roughly equal $k_B T$. The parameters $\tilde{\omega}_k'$ and $\tilde{\Gamma}_k$ correspond to the quasiparticle phonon frequency and linewidth at T. We use symbols with tildes on top to emphasize that they are obtained nonperturbatively through MD and are to be distinguished from ω_k' and Γ_k determined by PT.

To connect the results from MD with PT, one needs to establish a relation between the classical correlation functions and the quantum Green's functions. Using the Kubo transform,[29] the one-phonon Green's function can be written as $G_R(k,t) = -\beta \langle \tilde{v}_k^\dagger(0) u_k(t) \rangle \theta(t)$, where $\tilde{v}_k^\dagger = \frac{1}{\beta} \int_0^\beta d\lambda e^{\lambda H} v_k^\dagger e^{-\lambda H}$. In the classical limit, where $\beta = 1/(k_B T)$ approaches 0, $G_R(k,t)$ becomes its classical counterpart G_C

$$G_C(k,t) = -\beta \langle v_k^*(0) u_k(t) \rangle \theta(t) \tag{11}$$

or in the frequency domain

$$G_C(k,\omega) = -\beta \langle v_k^* u_k \rangle_\omega = \frac{\beta}{i\omega} \langle v_k^* v_k \rangle_\omega. \tag{12}$$

The left-hand side of Eq. (12) can be approximated with PT using Eqs. (7) and (8). The right-hand side can be obtained from MD. Equation (12) enables us to compare the PT and MD results in the whole frequency range.

When the frequency dependence of $\Sigma(k,\omega)$ is weak, and both the frequency shift $\Sigma_1(k,\omega_k) = \Delta_k$ and phonon linewidth $\Sigma_2(k,\omega_k) = -\Gamma_k$ are small, Eq. (7) can be simplified as

$$G_C(k,\omega) \approx -\frac{1}{\omega_k'} \left[\frac{\omega_k'}{\omega_k'^2 - (\omega + i\Gamma_k)^2} \right], \tag{13}$$

where $\omega_k' = \omega_k + \Delta_k$ is the phonon quasiparticle frequency. The expression in the bracket is the Fourier transform of the function $\sin(\omega_k' t) e^{-\Gamma_k t} \theta(t)$. From Eqs. (11) and (13) we see when $t > 0$ the classical correlation function

$$\langle v_k^*(0) u_k(t) \rangle \approx \frac{k_B T}{\omega_k'} \sin(\omega_k' t) e^{-\Gamma_k t}. \tag{14}$$

From Eq. (10) and Eq. (14) we get the approximate expressions for the other two correlations as

$$\langle v_k^*(0) v_k(t) \rangle \approx k_B T \cos(\omega_k' t) e^{-\Gamma_k t},$$

$$\langle u_k^*(0) u_k(t) \rangle \approx \frac{k_B T}{\omega_k'^2} \cos(\omega_k' t) e^{-\Gamma_k t}. \tag{15}$$

This justifies the phenomenological approach of fitting $\langle v_k^*(0) v_k(t) \rangle$ with a function $A_k \cos(\tilde{\omega}_k' t) e^{-\tilde{\Gamma}_k t}$. As we will show later, this simplified approach works well for phonon modes whose $\Sigma(k,\omega)$ is small and shows little frequency dependence near the resonant frequency ω_k. However, there are situations where $\Sigma(k,\omega)$ changes rapidly near ω_k. For such cases we resort to Eq. (12) to compare PT and MD.

We carry out molecular-dynamics simulations using a *NVE* ensemble on a rhomboid 16×16 supercell containing 256 particles. The initial velocity and displacement of each particle is set by a random number generator. Temperature is

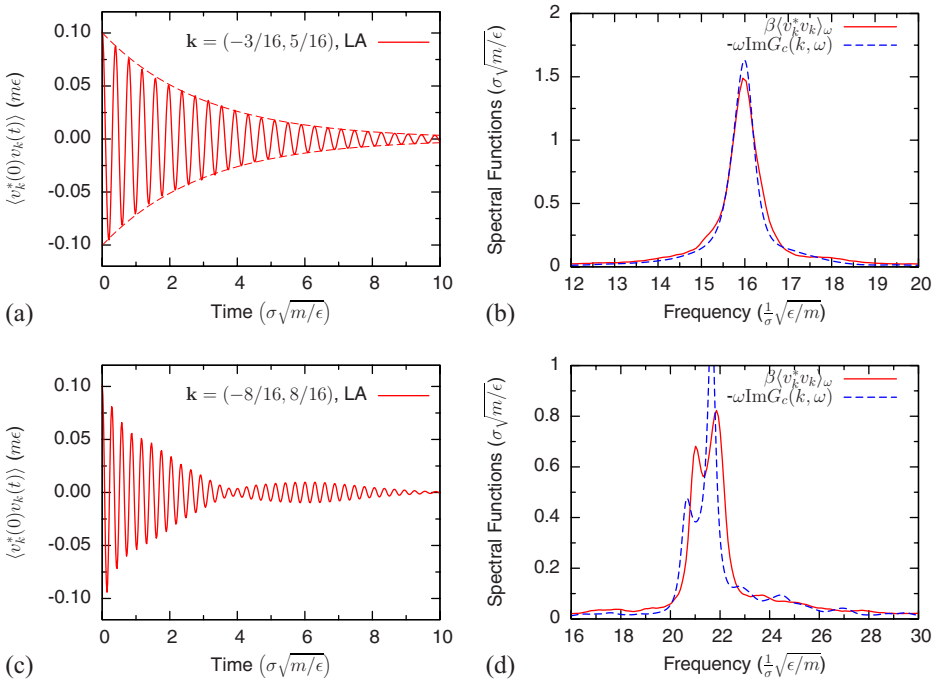

FIG. 5. (Color online) (a) Correlation functions $\langle v_k^*(0)v_k(t)\rangle$ obtained from MD for the longitudinal mode of $\mathbf{k}=(-3/16,5/16)$ at $T=0.1$. (b) Fourier spectrum $\langle v_k^* v_k\rangle_\omega$ of the correlation function shown in (a), compared with the Green's function computed by PT. (c) Correlation functions $\langle v_k^*(0)v_k(t)\rangle$ obtained from MD for the longitudinal mode of $\mathbf{k}=(-8/16,8/16)$ at $T=0.1$. (d) Fourier spectrum of the correlation function shown in (c), compared with the Green's function computed by PT.

defined as the average kinetic energy of the particles and velocity rescaling is used in the first few steps to let the system reach the desired temperature. The temperature range is set from $T=0.05$ to 0.9. Theoretically the melting point of a 2D LJ triangular lattice is about 1.4.[30] In our model each particle interacts with only its six designated first neighbors. When $T>1.0$ some particles will have sufficient kinetic energy to climb out of the potential well and the system becomes disordered. A velocity-Verlet algorithm[31] is used to integrate the equation of motion. The time step Δt is 0.001. The system first runs for hundreds of time units to reach equilibrium, then evolves further (from 5000 time units for $T=0.8$ to 40 000 for $T=0.05$. Using the LJ units of inert gas Ar, these correspond to 12.6 ns and 100.6 ns, respectively) for production. In the production stage, the normal-mode coordinates u_k and v_k are computed at every 10 time steps using fast Fourier transform. Usually the correlation function $\langle v_k^*(0)v_k(t)\rangle$ fits well to a function $A_k \cos(\tilde{\omega}_k' t)e^{-\tilde{\Gamma}_k t}$. The fitting errors (reduced χ^2) are typically less than 10^{-4}. We repeat the simulation with different initial configurations and estimate that the error in the fitted phonon quasiparticle frequency $\tilde{\omega}_k'$ is less than 1%. The error in the phonon linewidth $\tilde{\Gamma}_k$ is higher, around 5%.

It is tedious to calculate for each phonon mode its self-energy $\Sigma(k,\omega)$ from Eq. (8) and the correlation function $\langle v_k^*(0)v_k(t)\rangle$ from MD. Redundant work is avoided by noticing that the 2D triangular lattice has a symmetry of C_{6v}. For our 16×16 supercell, among the 512 modes, only 60 modes are independent. We study the phonon properties within the irreducible Brillouin zone, then combine them with appropriate symmetry factors when summing over the whole Brillouin zone.

Figure 5(a) shows the correlation function $\langle v_k^*(0)v_k(t)\rangle$ of the longitudinal mode of $\mathbf{k}=(-3/16,5/16)$ obtained from MD at $T=0.1$. This function fits very well to $A_k \cos(\tilde{\omega}_k' t)e^{\tilde{\Gamma}_k t}$. Accordingly, its Fourier transform $\langle v_k^* v_k\rangle_\omega$, shown in Fig. 5(b), has a nice Lorentzian line shape. We find such Lorentzian-type fittings work well for most vibrational modes, especially at higher T when $\langle v_k^*(0)v_k(t)\rangle$ decays faster. In such cases $\langle v_k^* v_k\rangle_\omega$ has a broader line shape, which tends to smear out detailed features. However, we also encounter more complex situations, as shown in Fig. 5(c). This correlation function, obtained from MD at $T=0.1$ for the longitudinal mode of $\mathbf{k}=(-8/16,8/16)$ (corresponding to the **M** point of the Brillouin zone), cannot be fitted satisfactorily in the same way as $\mathbf{k}=(-3/16,5/16)$. Its Fourier spectrum, shown in Fig. 5(d), contains a "double-peak" feature. There is no quasiparticle frequency and linewidth for this particular mode. This is similar to the measured Raman mode of CuCl at low T.[32,33] At high T the CuCl Raman "mode" broadens and acquires even more substructures. In our system very few phonons share such complexities. Usually the main character of a phonon k at T is well captured with two simple parameters, $\tilde{\omega}_k'$ and $\tilde{\Gamma}_k$.

Anharmonic PT provides valuable insights into the behaviors of the correlation functions described above. Figures 5(b) and 5(d) include the imaginary parts of the Green's functions in the classical limit $\mathrm{Im}\, G_C(k,\omega)$ evaluated from Eqs. (7) and (8). From Eq. (12) we know $-\omega\, \mathrm{Im}\, G_C(k,\omega)$ and $\beta\langle v_k^* v_k\rangle_\omega$ should be identical, if both are evaluated exactly. Since the phonon self-energy is evaluated only to lowest order, the two functions differ. The spectral function $-\omega\, \mathrm{Im}\, G_C(k,\omega)$ for the LA mode of $\mathbf{k}=(-3/16,5/16)$ has a Lorentzian line shape and agrees well with the corresponding $\beta\langle v_k^* v_k\rangle_\omega$. The quantitative agreement between the two functions is less impressive for $\mathbf{k}=(-8/16,8/16)$. However, $-\omega\, \mathrm{Im}\, G_C(k,\omega)$ also contains the double-peak feature observed in $\beta\langle v_k^* v_k\rangle_\omega$. The origin of this feature can be understood from the phonon self-energy spectra. As shown in Fig. 6, $\Sigma(k,\omega)$ for the LA mode of $\mathbf{k}=(-3/16,5/16)$ is quite flat near its resonant frequency, which enables us to ignore the

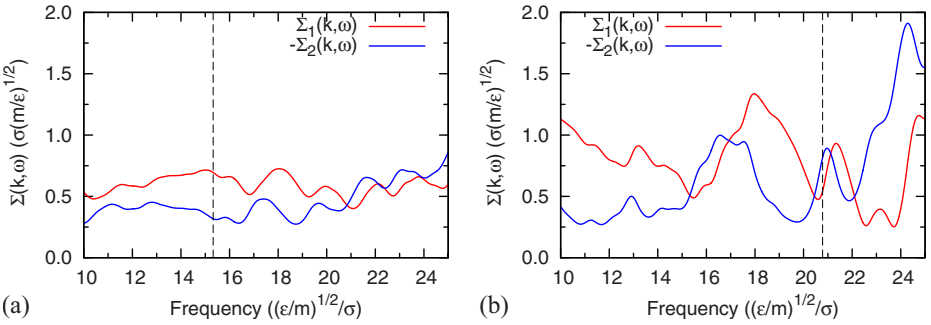

FIG. 6. (Color online) Phonon self-energy $\Sigma(k,\omega)$ evaluated by using Eq. (8) at $T=0.1$. (a) Longitudinal mode of $\mathbf{k}=(-3/16,5/16)$ and (b) longitudinal mode of $\mathbf{k}=(-8/16,8/16)$.

frequency dependence of $\Sigma(k,\omega)$ and approximate $G_C(k,\omega)$ with a Lorentzian function. In contrast, the LA mode of $\mathbf{k}=(-8/16,8/16)$ has a $\Sigma(k,\omega)$ varying abruptly near the resonant frequency. The frequency dependence of $\Sigma(k,\omega)$ can no longer be ignored and the double-peak feature appears in $\langle v_k^* v_k \rangle_\omega$.

Figure 7 shows the phonon quasiparticle frequency shifts and line widths determined by MD and by PT. At $T=0.1$ they agree very well. This observation is consistent with previous studies on similar systems.[4,6]

Figure 8 shows the temperature dependence of $\tilde{\omega}_k'$ and $\tilde{\Gamma}_k$ for the representative mode $\mathbf{k}=(-3/16,5/16)$. At low T both $\tilde{\omega}_k'$ and $\tilde{\Gamma}_k$ show good linear T dependence, in agreement with the lowest order PT. However, noticeable deviations, roughly quadratic in T, are observed at high T. Similar quadratic deviations are observed for other modes. Since $\tilde{\omega}_k'$ and $\tilde{\Gamma}_k$ are evaluated nonperturbatively, deviations from linear in T correspond to higher order anharmonic effects. In the next section we discuss how the T dependence of the phonon quasiparticle spectra affects the thermal properties of the system.

VI. THERMAL PROPERTIES

A. Mean-square displacement

We first consider the mean-square displacement (MSD). It is related to the Debye-Waller factor in diffraction experiments and often serves as an indicator of the solid-liquid phase transition.[34] In MD simulations, it is evaluated by averaging over the displacements of all particles at every time step, $\langle u^2(t)\rangle=(1/N)\Sigma_i u_i^2(t)$, then taking the time average. Harmonic (HA) theory predicts that MSD is linear in T, as shown in Eq. (5). Anharmonicity causes deviations from this linear T dependence. The lowest order anharmonic correction is proportional to phonon frequency shifts[35]

$$\langle u^2\rangle = \frac{k_B T}{Nm}\sum_k \frac{1}{\omega_k^2}\left(1-2\frac{\Delta_k}{\omega_k}\right). \tag{16}$$

Since Δ_k is linear in T to the first order, the leading-order anharmonic correction to $\langle u^2\rangle$ is quadratic in T.

Figure 9 compares MSD obtained from direct MD simulations, from harmonic phonon spectra using Eq. (5) and from the lowest order anharmonic perturbation theory using Eqs. (8) and (16). We find that exact MD results are not far from the linear T relation predicted by harmonic theory and the lowest order anharmonic correction from Eq. (16) is sufficient to account for most of the differences between the exact MD results and HA results. Anharmonic PT works surprisingly well in predicting the MSD of our system.

B. Thermal pressure

Thermal pressure is a fundamental thermal property of materials. Accurate determination of thermal pressure is crucial to establish reliable pressure scales used in high-T high-P experiments,[36] and to determine phase-transition boundaries precisely.[16] A comparison of $P(T)$ obtained from MD, from QHA, and from anharmonic PT is particularly important. There are standard formulas to calculate thermal pressure in MD simulations. For our 2D system consisting of particles interacting with pair-wise potential $\phi(r_{ij})$ (Ref. 31)

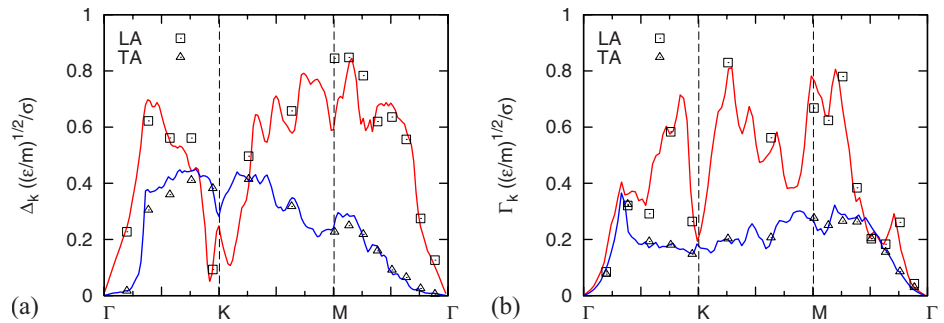

FIG. 7. (Color online) (a) Frequency shift and (b) phonon linewidth, obtained at $T=0.1$ by perturbation theory (solid lines) compared with those from molecular dynamics (squares and triangles). PT results are obtained by evaluating Eq. (8) for each k; MD results are obtained by fitting the correlation functions $\langle v_k^*(0)v_k(t)\rangle$ with $A_k\cos(\tilde{\omega}_k' t)e^{\tilde{\Gamma}_k t}$.

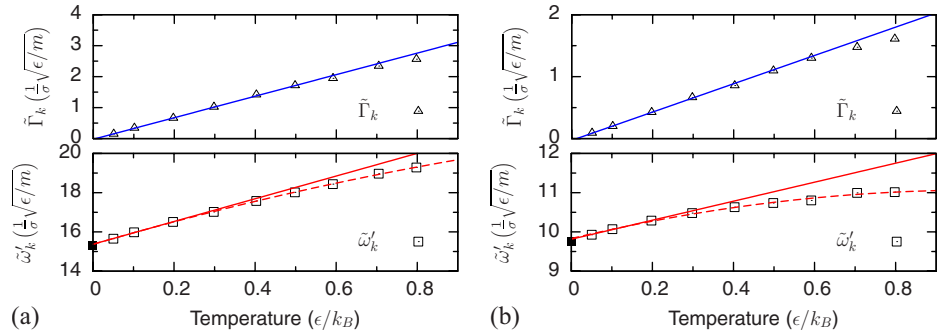

FIG. 8. (Color online) Temperature dependence of the phonon quasiparticle frequency $\tilde{\omega}'_k$ and linewidth $\tilde{\Gamma}_k$ obtained nonperturbatively through MD at $\mathbf{k}=(-3/16,5/16)$. (a) Longitudinal mode and (b) transverse mode. The solid straight lines correspond to the linear fits in the range $T\leq 0.2$. The dashed curves in the T-$\tilde{\omega}'_k$ subfigures correspond to quadratic fits.

$$PA = Nk_BT - \frac{1}{2}\left\langle \frac{1}{2}\sum_i \sum_j r_{ij}\phi'(r_{ij}) \right\rangle, \tag{17}$$

where the term in the $\langle \ldots \rangle$ is the virial function. In QHA, $P(T)$ is related to the quasiparticle entropy through the Maxwell relation $(\partial P/\partial T)_V=(\partial S/\partial V)_T$, from which $P(T)$ is represented in term of the mode-Grüneisen parameters as

$$P_{\mathrm{QH}}(T) = \frac{k_BT}{A}\sum_k \gamma_k. \tag{18}$$

The leading correction given by anharmonic PT is[9]

$$P(T) = \frac{k_BT}{A}\sum_k \left(\gamma_k - \frac{A}{2\omega_k}\frac{\partial \Delta_k}{\partial A}\right), \tag{19}$$

where $\partial\Delta_k/\partial A$ corresponds to the volume dependence of the frequency shift. We calculate Δ_k using Eq. (8) for both the original cell and a slightly expanded (0.2%) cell, then compute $\partial\Delta_k/\partial A$ by finite difference. Similar to MSD, the leading-order anharmonic correction to $P(T)$ is also quadratic in T.

Figure 10 shows $P(T)$ evaluated by the three methods. At $T<0.3$, the exact $P(T)$ obtained from MD is close to linear in T and agrees with the QHA prediction. Considerable deviations from the linear T relation are observed at high T, which are largely accounted for by the leading-order anharmonic correction defined in Eq. (19). Thus thermal pressure $P(T)$ of our system is well described by anharmonic PT.

C. Free energy, entropy, and heat capacity

Unlike MSD and $P(T)$, thermal properties such as free energy and entropy are not directly accessible in *NVE* molecular-dynamics simulations. However, one can choose the harmonic system as a reference and use thermodynamic integration[31] to obtain the exact anharmonic free energy $F_{\mathrm{A}}(T)=F(T)-F_{\mathrm{H}}(T)$,

$$\frac{F_{\mathrm{A}}(T)}{N} = -k_BT\int_0^T \frac{dT'}{T'}\left\{\frac{[E(T')-E_0]-[E_{\mathrm{H}}(T')-E_0]}{Nk_BT'}\right\}$$
$$= -k_BT\int_0^T \frac{dT'}{T'}\left[\frac{E(T')-E_0}{Nk_BT'}-2\right], \tag{20}$$

where $E(T')$ is the total energy of the system, fixed in a *NVE* molecular-dynamics run so that the system's average temperature is T'. $E_{\mathrm{H}}(T')$ is the total energy of the harmonic system, $E_0=-3N\epsilon$ is the ground-state energy. For our 2D model, $E_{\mathrm{H}}(T')-E_0$ equals $2Nk_BT'$. We use a fourth-order polynomial of T' to fit $[E(T')-E_0]/(Nk_BT')$, then integrate it to get $F_{\mathrm{A}}(T)$.[5] The anharmonic part of the entropy $S-S_{\mathrm{H}}=S_{\mathrm{A}}$ is calculated from $S_{\mathrm{A}}=-\partial F_{\mathrm{A}}/\partial T$. The heat capacity C_V

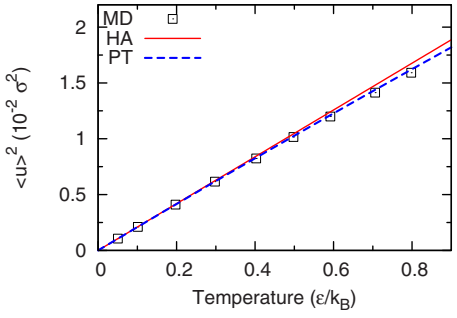

FIG. 9. (Color online) Mean-square displacement. Squares labeled as "MD" denote data from direct MD simulations. The solid red line labeled as "HA" denote the results predicted from harmonic phonon spectra via Eq. (5). The dashed blue line labeled as "PT" corresponds to results obtained from the lowest order anharmonic perturbation theory via Eq. (16).

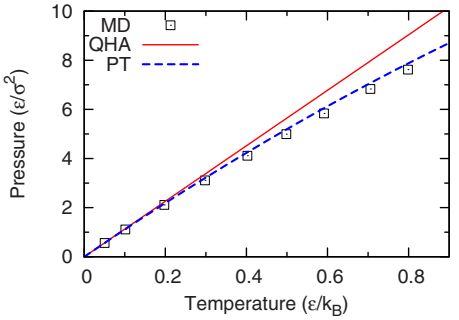

FIG. 10. (Color online) Thermal pressure $P(T)$ at fixed volume. Squares labeled as MD denote data from direct MD simulations using Eq. (17). The solid red line labeled as QHA denote the results predicted within QHA using Eq. (18). The dashed blue line labeled as PT corresponds to anharmonic PT predictions from Eq. (19).

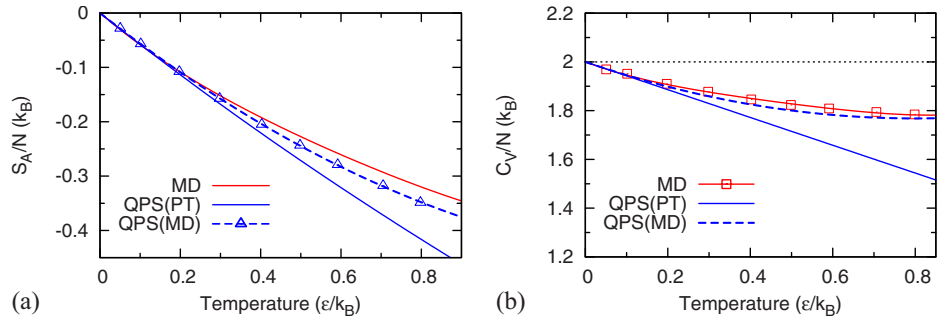

FIG. 11. (Color online) Thermal properties computed by direct MD simulations and by formulas based on phonon spectra. (a) Anharmonic entropy. The solid red line labeled as MD denotes S_A obtained from thermodynamical integration, corresponding to the exact results. The solid blue line labeled as "QPS(PT)" corresponds to results obtained from phonon QPS determined by the lowest order perturbation theory. Triangles labeled as "QPS(MD)" denote data from QPS determined nonperturbatively through MD. The dashed blue line corresponds to a quadratic fit to these discrete data points. (b) Heat capacity at constant volume. Squares labeled as MD denote C_V determined from the fluctuations of the kinetic energy in the MD simulations. The solid red line denotes C_V obtained from thermodynamic integration and corresponds to S_A with the same symbol in (a). The same correspondence holds for quantities labeled as QPS(PT) and QPS(MD).

is from $C_V/N=2k_B-(T/N)\partial S_A/\partial T$. Another way to evaluate C_V is from the fluctuation of the kinetic energy.[37] Denote the average total kinetic energy of the system as K, its variance as δK, for our 2D system we have $C_V/N=k_B(1-N(\delta K)^2/\langle K\rangle^2)^{-1}$. The C_V obtained by the two methods agree within a few percent.

From the quasiparticle entropy formula Eq. (1) one finds that S_A is represented in terms of phonon quasiparticle frequencies as

$$\frac{S_A}{N}=-\frac{k_B}{N}\sum_k \ln\frac{\omega_k'}{\omega_k}\approx-\frac{k_B}{N}\sum_k\frac{\Delta_k}{\omega_k}. \tag{21}$$

The leading anharmonic correction to S_A is linear in T, one power less than the corrections to MSD and $P(T)$. The corresponding formula for heat capacity C_V is

$$\frac{C_V}{N}=\frac{k_B}{N}\sum_k\left(1-\frac{T}{\omega_k}\frac{\partial\Delta_k}{\partial T}\right). \tag{22}$$

The leading anharmonic correction to C_V is also linear in T.

Figure 11 shows S_A and C_V computed by direct MD simulations and those predicted by quasiparticle theory. With quasiparticle spectra (QPS) determined by the lowest order PT using Eq. (8), the formula for quasiparticle entropy correctly gives the leading anharmonic correction to S_A and C_V, which agree well with the exact MD data at low T. However, including only the leading anharmonic corrections become inadequate at higher T, especially for C_V. Because C_V is defined as $T\partial S/\partial T$ and if S is a polynomial of T, then a T^n term in S is enhanced by a factor of n in C_V. Thus C_V is more sensitive to higher order effects.

We try to capture some higher order anharmonic effects by substituting the nonperturbative phonon frequencies $\tilde{\omega}_k'$ into Eq. (21). The results are shown in Fig. 11 with the label "QPS(MD)." Comparing to the results obtained from PT [labeled as "QPS(PT)"] via Eqs. (8), (21), and (22), using nonperturbative phonon frequencies improves the agreements with the exact MD data considerably. From previous discussions we know that $\tilde{\omega}_k'$ is nearly linear in T and agrees well with PT at low T. At $T>0.3$, $\tilde{\omega}_k'$ shows an extra quadratic T dependence due to higher order anharmonic interactions. Accordingly, using the nonperturbative phonon frequencies in the quasiparticle entropy formula yields the same leading anharmonic correction at low T. Further more, it captures a large portion of higher order anharmonic effects at high T. Quasiparticle theory, not limited to the lowest order, works quite well in predicting the thermal properties of our model system. This is in contrast with the study of thermal conductivity of the same system in paper II,[3] where quasiparticle theory fails to predict the correct thermal conductivity, even with the exact phonon relaxation times.

VII. CONCLUSIONS

We use MD to assess the validity of phonon quasiparticles and anharmonic PT on a 2D triangular model system. The phonon quasiparticle spectra were obtained both by leading-order PT and nonperturbatively by MD. Good agreement between the two is observed at low T while noticeable deviations show up at high T due to higher order anharmonic interactions. Substituting the quasiparticle frequencies obtained by leading-order PT into the quasiparticle entropy formula correctly produces the first-order anharmonic corrections to the thermal properties. If one uses the quasiparticle frequencies obtained nonperturbatively by MD, then higher order anharmonic corrections are also described. In contrast to thermal conductivity discussed in II,[3] quasiparticle theory is surprisingly successful in predicting the thermodynamics of our model system.

ACKNOWLEDGMENTS

We thank Julie Stern for help with early computations. Early work at Stony Brook was supported in part by NSF ITR under Grant No. ATM0426757. Recent work at Stony Brook was funded by DOE under Grant No. DE-FG02-08ER46550.

APPENDIX: POTENTIAL EXPANSIONS

At $r-\sigma$ less than the radius of convergence $|r-\sigma|=\sigma$, the interparticle potential $\phi_{\mathrm{LJ}}(r)$ can be expanded around $r=\sigma$ in a power series of the relative displacements, $\mathbf{u}_{ij}=\mathbf{r}_{ij}-\mathbf{R}_{ij}$.[38]

$$\phi(r_{ij}) = \phi(R_{ij}) + \phi^{(1)} + \phi^{(2)} + \phi^{(3)} + \phi^{(4)} + \cdots, \quad \text{(A1)}$$

where

$$\phi^{(1)} = \sum_{\alpha} \frac{\partial \phi}{\partial r_{i\alpha}} u_{ij\alpha},$$

$$\phi^{(2)} = \frac{1}{2!} \sum_{\alpha\beta} \frac{\partial^2 \phi}{\partial r_{i\alpha}\, \partial r_{i\beta}} u_{ij\alpha} u_{ij\beta},$$

$$\phi^{(3)} = \frac{1}{3!} \sum_{\alpha\beta\gamma} \frac{\partial^3 \phi}{\partial r_{i\alpha}\, \partial r_{i\beta}\, \partial r_{i\gamma}} u_{ij\alpha} u_{ij\beta} u_{ij\gamma},$$

$$\phi^{(4)} = \frac{1}{4!} \sum_{\alpha\beta\gamma\sigma} \frac{\partial^4 \phi}{\partial r_{i\alpha}\, \partial r_{i\beta}\, \partial r_{i\gamma}\, \partial r_{i\sigma}} u_{ij\alpha} u_{ij\beta} u_{ij\gamma} u_{ij\sigma}. \quad \text{(A2)}$$

The potential derivatives are defined as $\partial\phi/\partial r_{i\alpha} = (\phi'/R_{ij}) R_{ij\alpha}$, $\partial^2\phi/\partial r_{i\alpha}\partial r_{i\beta} = (\phi''-\phi'/R_{ij})(R_{ij\alpha}R_{ij\beta}/R_{ij}^2) + (\phi'/R_{ij})\delta_{\alpha\beta}$, etc.[15] Accordingly, the total potential Φ is expanded as

$$\Phi = \Phi^{(0)} + \Phi^{(2)} + \Phi^{(3)} + \Phi^{(4)} + \cdots, \quad \text{(A3)}$$

where $\Phi^{(0)}$ is the classical ground-state energy $-3N\epsilon$. The linear term in the displacements $\Phi^{(1)}$ is zero for the equilibrium lattice. The second-order term

$$\Phi^{(2)} = \frac{1}{2} \sum_i \sum_j \phi^{(2)}(r_{ij}) = \frac{1}{4} \sum_i \sum_j \sum_{\alpha\beta} \frac{\partial^2 \phi}{\partial r_{i\alpha}\, \partial r_{i\beta}} u_{ij\alpha} u_{ij\beta} \quad \text{(A4)}$$

determines the harmonic phonon spectrum. For the 2D triangular lattice model, where each atom interacts only with six nearest atoms, the dynamical matrix

$$\mathcal{D}_{\alpha\beta}(\mathbf{k}) = 4 \sum_{\mathbf{R}=\mathbf{a},\mathbf{b},\mathbf{c}} \left[\left(\phi'' - \frac{\phi'}{R} \right) \frac{R_\alpha R_\beta}{R^2} + \frac{\phi'}{R} \delta_{\alpha\beta} \right] \sin^2\left(\frac{\mathbf{k}\cdot\mathbf{R}}{2} \right). \quad \text{(A5)}$$

The vibrational normal modes are determined by the eigenvectors of $\mathcal{D}_{\alpha\beta}(\mathbf{k})$, denoted as $\hat{\mathbf{e}}_k$. The eigenvalues of $\mathcal{D}_{\alpha\beta}$, which are squared frequencies $\lambda_\pm = m\omega_\pm^2(\mathbf{k})$, can be written in the symmetric form

$$\lambda_\pm = 2\left(\phi'' + \frac{\phi'}{R} \right)(s_a + s_b + s_c) \pm 2\left(\phi'' - \frac{\phi'}{R} \right) \times \sqrt{s_a^2 + s_b^2 + s_c^2 - s_a s_b - s_b s_c - s_c s_a}, \quad \text{(A6)}$$

where $s_a = \sin^2(\mathbf{k}\cdot\mathbf{a}/2)$, and similarly for s_b and s_c. Even though $\phi'=0$ in our constant volume calculations, still we keep the full expression because it will be used for the calculation of the mode-Grüneisen parameter.

The mode-Grüneisen parameter is defined as

$$\gamma_k = -\left(\frac{\partial \ln \omega_k}{\partial \ln V} \right)_T. \quad \text{(A7)}$$

For our 2D model, V is replaced by area A

$$\gamma_k = -\frac{\partial \ln \omega_k}{\partial \ln A} = -\frac{A}{2\omega_k^2}\frac{d\omega_k^2}{dA} = \frac{1}{4}\left(\frac{\phi'''}{\phi''} R - 1 \right) - \frac{1}{2} \frac{s_a + s_b + s_c}{(s_a + s_b + s_c) \pm \sqrt{s_a^2 + s_b^2 + s_c^2 - s_a s_b - s_b s_c - s_c s_a}}. \quad \text{(A8)}$$

The anharmonic phonon-phonon interactions are determined by normal-mode transform

$$\mathbf{u}_i = \frac{1}{\sqrt{Nm}} \sum_k u_k \hat{\mathbf{e}}_k e^{i\mathbf{k}\cdot\mathbf{R}_i} \quad \text{(A9)}$$

such that

$$\Phi^{(3)} = \frac{1}{2} \sum_i \sum_j \phi^{(3)}(r_{ij}) = \sum_{k_1 k_2 k_3} \Phi_3(k_1 k_2 k_3) u_{k_1} u_{k_2} u_{k_3},$$

$$\Phi^{(4)} = \frac{1}{2} \sum_i \sum_j \phi^{(4)}(r_{ij}) = \sum_{k_1 k_2 k_3 k_4} \Phi_4(k_1 k_2 k_3 k_4) u_{k_1} u_{k_2} u_{k_3} u_{k_4}, \quad \text{(A10)}$$

where

$$\Phi_3(k_1 k_2 k_3) = \frac{1}{12} \frac{1}{\sqrt{Nm^3}} \sum_j \sum_{\alpha\beta\gamma} \frac{\partial^3 \phi}{\partial r_{i\alpha}\, \partial r_{i\beta}\, \partial r_{i\gamma}} \times \hat{e}_\alpha(k_1) \hat{e}_\beta(k_2) \hat{e}_\gamma(k_3) (1 - e^{-i\mathbf{k}_1\cdot\mathbf{R}_{ij}})(1 - e^{-i\mathbf{k}_2\cdot\mathbf{R}_{ij}}) \times (1 - e^{-i\mathbf{k}_3\cdot\mathbf{R}_{ij}}) \delta_{\mathbf{G}}(\mathbf{k}_1 + \mathbf{k}_2 + \mathbf{k}_3),$$

$$\Phi_4(k_1 k_2 k_3 k_4) = \frac{1}{48} \frac{1}{Nm^2} \sum_j \sum_{\alpha\beta\gamma\sigma} \times \frac{\partial^4 \phi}{\partial r_{i\alpha}\, \partial r_{i\beta}\, \partial r_{i\gamma}\, \partial r_{i\sigma}} \hat{e}_\alpha(k_1) \hat{e}_\beta(k_2) \hat{e}_\gamma(k_3) \hat{e}_\sigma(k_4) \times (1 - e^{-i\mathbf{k}_1\cdot\mathbf{R}_{ij}})(1 - e^{-i\mathbf{k}_2\cdot\mathbf{R}_{ij}})(1 - e^{-i\mathbf{k}_3\cdot\mathbf{R}_{ij}})(1 - e^{-i\mathbf{k}_4\cdot\mathbf{R}_{ij}}) \delta_{\mathbf{G}}(\mathbf{k}_1 + \mathbf{k}_2 + \mathbf{k}_3 + \mathbf{k}_4). \quad \text{(A11)}$$

The subscript $\mathbf{G}$ on $\delta_{\mathbf{G}}(\mathbf{k})$ indicates that the argument must equal a reciprocal-lattice vector.

*tsun@grad.physics.sunysb.edu
†Present address: Department of Physics and Astronomy, Vanderbilt University, Nashville, Tennessee 37235, USA.
‡philip.allen@stonybrook.edu

[1] A. Ward and D. A. Broido, Phys. Rev. B **81**, 085205 (2010).
[2] B. Prevot, B. Hennion, and B. Dorner, J. Phys. C **10**, 3999 (1977).
[3] T. Sun and P. B. Allen, following paper, Phys. Rev. B **82**, 224305 (2010).
[4] A. J. C. Ladd, B. Moran, and W. G. Hoover, Phys. Rev. B **34**, 5058 (1986).
[5] D. J. Lacks and R. C. Shukla, Phys. Rev. B **54**, 3266 (1996).
[6] J. E. Turney, E. S. Landry, A. J. H. McGaughey, and C. H. Amon, Phys. Rev. B **79**, 064301 (2009).
[7] L. D. Landau and E. M. Lifshitz, *Statistical Physics* (Butterworth-Heinemann, London, 1980).
[8] T. H. K. Barron, in *Lattice Dynamics*, edited by R. F. Wallis (Pergamon, New York, 1965), p. 247.
[9] D. C. Wallace, *Thermodynamics of Crystals* (Wiley, New York, 1972).
[10] G. Grimvall, *Thermophysical Properties of Materials* (North-Holland, Amsterdam, 1999).
[11] J. C. K. Hui and P. B. Allen, J. Phys. C **8**, 2923 (1975).
[12] A. R. Oganov and P. I. Dorogokupets, J. Phys.: Condens. Matter **16**, 1351 (2004).
[13] M. H. G. Jacobs and B. H. W. S. de Jong, Phys. Chem. Miner. **32**, 614 (2005).
[14] B. B. Karki, R. M. Wentzcovitch, S. de Gironcoli, and S. Baroni, Science **286**, 1705 (1999).
[15] R. A. Cowley, Adv. Phys. **12**, 421 (1963); Rep. Prog. Phys. **31**, 123 (1968).
[16] Z. Wu and R. M. Wentzcovitch, Phys. Rev. B **79**, 104304 (2009).
[17] R. E. Peierls, Ann. Physik **3**, 1055 (1929).
[18] W. Pauli, in *Collected Scientific Papers*, edited by R. Kronig and V. Weisskopf (Wiley, New York, 1964), p. 549.
[19] G. Grosso and G. P. Parravicini, *Solid State Physics* (Academic, San Diego, 2000), p. 204.
[20] M. Born, Math. Proc. Cambridge Philos. Soc. **36**, 160 (1940).
[21] J. B. Lurie, J. Low Temp. Phys. **10**, 751 (1973).
[22] L. D. Landau, Phys. Z. Sowjetunion **11**, 26 (1937).
[23] R. E. Peierls, Helv. Phys. Acta **7**, 81 (1923); Ann. Inst. Henri Poincare **5**, 177 (1935).
[24] N. D. Mermin, Phys. Rev. **176**, 250 (1968).
[25] Y. Imry and L. Gunther, Phys. Lett. A **29**, 483 (1969).
[26] A. A. Maradudin and A. E. Fein, Phys. Rev. **128**, 2589 (1962).
[27] J. P. Hansen and I. R. McDonald, *Theory of Simple Liquids* (Elsevier, London, 2006).
[28] N. de Koker, Phys. Rev. Lett. **103**, 125902 (2009).
[29] R. Kubo, J. Phys. Soc. Jpn. **12**, 570 (1957).
[30] J. Dietel and H. Kleinert, Phys. Rev. B **73**, 024113 (2006).
[31] M. P. Allen and D. J. Tildesley, *Computer Simulation of Liquids* (Oxford University Press, Oxford, 1987).
[32] J. E. Potts, R. C. Hanson, C. T. Walker, and C. Schwab, Phys. Rev. B **9**, 2711 (1974).
[33] M. Krauzman, R. M. Pick, H. Poulet, G. Hamel, and B. Prevot, Phys. Rev. Lett. **33**, 528 (1974).
[34] C. Kittel, *Introduction to Solid State Physics*, 7th ed. (Wiley, New York, 1996).
[35] R. C. Shukla and H. Hübschle, Phys. Rev. B **40**, 1555 (1989).
[36] T. Sun, K. Umemoto, Z. Wu, J.-C. Zheng, and R. M. Wentzcovitch, Phys. Rev. B **78**, 024304 (2008).
[37] J. L. Lebowitz, J. K. Percus, and L. Verlet, Phys. Rev. **153**, 250 (1967).
[38] A. A. Maradudin, P. A. Flinn, and R. A. Coldwell-Horsfall, Ann. Phys. **15**, 337 (1961); **15**, 360 (1961).